Giant magnetization canting due to symmetry breaking in zigzag Co chains on Ir(001)

2015 New J. Phys. 17 023014

(http://iopscience.iop.org/1367-2630/17/2/023014)

New Journal of Physics
The open access journal at the forefront of physics

Deutsche Physikalische Gesellschaft DPG
IOP Institute of Physics

Published in partnership with: Deutsche Physikalische Gesellschaft and the Institute of Physics

OPEN ACCESS

RECEIVED
23 September 2014

REVISED
22 December 2014

ACCEPTED FOR PUBLICATION
5 January 2015

PUBLISHED
4 February 2015

PAPER

Giant magnetization canting due to symmetry breaking in zigzag Co chains on Ir(001)

B Dupé[1], J E Bickel[2,4], Y Mokrousov[3], F Otte[1], K von Bergmann[2], A Kubetzka[2], S Heinze[1] and R Wiesendanger[2]

[1] Institute of Theoretical Physics and Astrophysics, Christian-Albrechts University of Kiel, Leibnizstrasse 15, D-24098 Kiel, Germany
[2] Institute of Applied Physics, Hamburg University, Jungiusstrasse 11, D-20355 Hamburg, Germany
[3] Peter Grünberg Institut and Institute for Advanced Simulation, Forschungszentrum Jülich and JARA, D-52425 Jülich, Germany
[4] Current address: Cleveland State University, Department of Physics, Cleveland, OH 44106, USA

E-mail: dupe@theo-physik.uni-kiel.de, and jbickel@mtholyoke.edu

Keywords: spin polarized STM, first principle calculations, magnetism

Abstract

We demonstrate a canted magnetization of biatomic zigzag Co chains grown on the (5 × 1) reconstructed Ir(001) surface using density functional theory (DFT) calculations and spin-polarized scanning tunneling microscopy (SP-STM) experiments. It is observed by STM that biatomic Co chains grow in three different structural configurations. Our DFT calculations show that they are all in a ferromagnetic (FM) state. Two chain types possess high symmetry due to two equivalent atomic strands and an easy magnetization direction that is along one of the principal crystallographic axes. The easy magnetization axis of the zigzag Co chains is canted away from the surface normal by an angle of 33°. This giant effect is caused by the broken chain symmetry on the substrate in combination with the strong spin–orbit coupling of Ir. SP-STM measurements confirm the stable FM order of the zigzag chains with a canted magnetization.

1. Introduction

Low-dimensional magnetic nanostructures on surfaces such as single atoms, clusters, and atomic chains constitute model systems to explore spintronic concepts at the ultimate scale. In view of their enhanced magnetocrystalline anisotropy energy (MAE), such nanomagnets are attractive for further miniaturization of data storage, as the MAE acts as a barrier and stabilizes the magnetization against thermal fluctuations. One of the most striking examples is the giant anisotropy reported for single-atom Co chains grown at the step edges of a Pt(111) surface, allowing the observation of ferromagnetic (FM) order [1]. Due to the step edge, the easy magnetization axis is not oriented along one of the high symmetry axes but it is canted from the surface normal by about 43° towards the upper Pt terrace [1], which is caused by the competition of contributions to the magnetocrystalline anisotropy from the Co and Pt atoms [2–4]. The addition of more atomic Co strands at the step edge reorients the magnetization direction away from the upper terrace and the direction oscillates until it is nearly perpendicular to the vicinal surface for a coverage of a monolayer [5, 6]. Since these pioneering experiments were performed, quasi-one-dimensional chains at surfaces have been the subject of intense research, in particular, in theoretical studies of magnetic structures on metal surfaces (e.g., [2–4, 6–13]) and metal structures on semiconductor surfaces [14, 15]. However, very few other systems have been characterized experimentally concerning their magnetic state [16–18].

One promising surface on which to grow quasi-one-dimensional chains is the (5 × 1) surface reconstruction of Ir(001) which exhibits a trench structure that allows self-assembly of different types of biatomic chains [19, 20]. Two of the chain configurations possess a high symmetry (i.e., do not break the symmetry of the Ir(001) (5 × 1) surface), with two equivalent atomic strands that adsorb either on the inner or outer hollow (OH) site of the trench (see figures 1(a) and (b)). For such biatomic Fe chains, it has been reported previously that due to the hybridization between Fe and Ir, the magnetic coupling and the easy magnetization axis depend significantly on

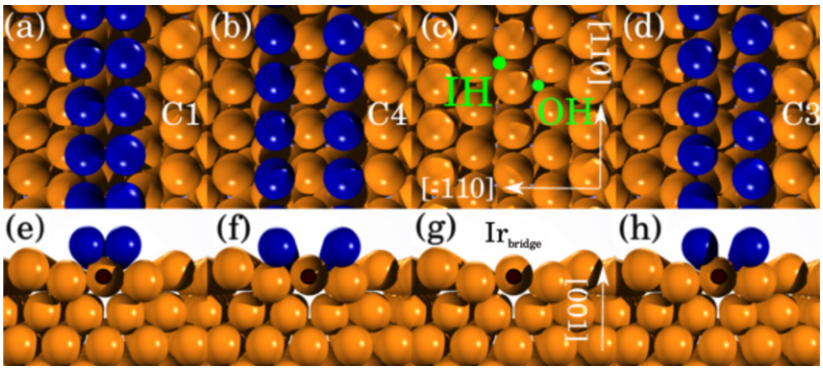

Figure 1. (a)–(d) Top and (e)–(h) side view of the three different chain configurations and the (5 × 1) reconstructed Ir(001) surface. In (c), the IH and OH sites and in (g) the bridge Ir atom are marked. For the C1 (a), (e) and C4 (b), (f) chains, the two strands are in the IH and OH sites, respectively, whereas for the C3 chain (d), (h), one is in the IH and the other in the OH site.

the adsorption site of the atoms [11, 12, 17]. If one of the two strands of the biatomic chain adsorbs on the inner hollow (IH) site while the other adsorbs on the OH site, a zigzag chain forms that breaks the [−110] mirror plane symmetry of the Ir(001)(5 × 1) surface and lowers the symmetry (see figures 1(c) and (d)). This type of chain has not been observed for Fe; however, as we show here, it can be formed by depositing Co.

In this paper, we demonstrate that the symmetry breaking of zigzag chains on a surface can lead to a giant canting of their easy magnetization direction. This is remarkable, since both the chain and the substrate separately possess high symmetry and exhibit a relatively small buckling when brought in contact with each other. It is in clear contrast to the case of atomic Co chains at a Pt(111) step edge where the surface structure already has broken symmetry and a canting of the magnetization is expected.

2. First-principles calculations

2.1. Computational details

We have performed density functional theory (DFT) calculations for biatomic Co chains on the (5 × 1) reconstructed Ir(001) surface, applying the film version of the full linearized augmented plane wave (FLAPW) method as implemented in the FLEUR code [21]. For all considered chains, we used a symmetric slab consisting of 37 Ir atoms (7 substrate layers) and 4 Co atoms. The resulting (5 × 1) supercell has inversion symmetry with Co chains on both surfaces. The setup of the (5 × 1) Ir(001) surface is the same as in [12], with biatomic chains lying along the [110] direction (see figure 1). In this configuration, the axes of the two adjacent chains are separated by 13.51 Å. We used the theoretical Ir lattice constant of 3.82 Å of [12] and muffin tin (MT) radii of $R_{\mathrm{MT}} = 2.1$ a.u. and $R_{\mathrm{MT}} = 2.3$ a.u. for Co and Ir atoms, respectively. The structural relaxation was carried out using a mixed LDA/GGA functional introduced by De Santis *et al* [22] to treat systems of 3*d*- and 5*d*-transition metals. The mixed functional considers the gradient correction in the interstitial region and in the MT spheres of the Co atoms and neglects it in the MT of the Ir. Therefore, the resulting functional treats the MT of Co and the interstitial region in generalized gradient approximation (GGA) [23], and the MT of Ir in local density approximation (LDA) [24]. Here, 24 k-points were used in a quarter of the Brillouin zone (BZ) for self-consistent calculations and geometry optimization. We used a cutoff parameter for the basis function $k_{\mathrm{max}} = 4.0$ a.u.$^{-1}$ for both relaxation and comparison of the total energies.

We calculated the MAE of the Co chains using the magnetic force theorem [25]. The convergence with respect to the k-point mesh, the basis set, and the energy window were carefully checked and 245 k-points in the full two-dimensional BZ, led to a precision of 0.1 meV sufficient for our system. Further tests involving 450 k-points in the full two-dimensional BZ, as well as an increase of the basis cutoff to ($k_{\mathrm{max}} = 4.1$ a.u.$^{-1}$), led to the same results. For the zigzag chains (C3 configuration), we have also checked several angles by self-consistent calculations including spin–orbit coupling and found energy differences very similar to those obtained with the force theorem.

2.2. Chain configurations and structure

We denote the biatomic chains with both atomic strands adsorbed in the IH or OH sites as C1 and C4, respectively [7], whereas the zigzag chain is referred to as the C3 chain (see figure 1). All structures were relaxed in the FM state. In the C1 and C4 configuration, the Co atoms and Ir atoms in the three upmost substrate layers were allowed to relax in all directions. For the C3 configuration, we relaxed the Co atoms in the vertical direction

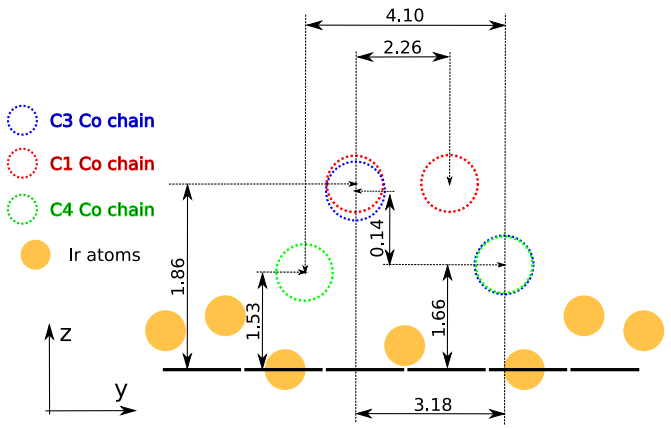

Figure 2. Schematic view of the relaxed configurations for the different biatomic Co chains. The top layer of the Ir substrate is also shown. For simplicity, the buckling of the Ir substrate, which is on the order of 0.05 Å in the case of the zigzag (C3) chains, is not shown. Note that in the sketch the atomic displacements are greatly exaggerated.

Table 1. Energy difference (in meV per Co atom) between the FM state and two AFM states. All the energies are given with respect to the C1-FM ground state configuration. In the configuration $AFM_{\|[110]}$, the magnetic moments of the atoms in the two strands are parallel, whereas they are antiparallel along the chain. In $AFM_{\|[\bar{1}10]}$, the moments in each strand are parallel, whereas the moments of the two strands are antiparallel to each other.

	C1	C3	C4
FM	0.00	30.8	52.3
$AFM_{\|[110]}$	77.3	137.3	148.3
$AFM_{\|[\bar{1}10]}$	192.8	42.3	58.5

and allowed the three upmost Ir layers to fully relax. A sketch of the chain geometries after structural relaxation is displayed in figure 2. Due to symmetry, the Co atoms stay in the IH and OH site in the symmetric C1 and C4 configurations, respectively, and display only a small lateral relaxation. In the C3 structure, we obtain a small vertical relaxation of the two strands and a vertical difference between them of 0.14 Å as well as a smaller buckling of the Ir substrate on the order of 0.05 Å.

The separation between the two Co strands increases as we move from the C1 to the C3 and to the C4 chain from 2.26 to 3.18 Å up to 4.10 Å. The magnetic moments of the Co atoms depend both on the hybridization between the two strands and of the strands with the Ir substrate. The resulting values for the Co atoms in C1 are 1.9 μ_B and decrease to 1.8 μ_B for the Co in the C4 configuration. For the C3 chains, the moments are comparable with the high symmetry configurations: 1.9 μ_B for the IH site atom and 1.8 μ_B for the OH site atom. The magnetic moment of the Ir atom at the bridge site is 0.25 μ_B in the C3 configuration and 0.3 μ_B and 0.1 μ_B in the C1 and C4 configuration, respectively. The magnetic moments of the Ir atoms with only one Co atom as nearest neighbor is of the order of 0.1 μ_B, and for the Ir atoms not adjacent to the Co chain, a magnetic moment of less than 0.05 μ_B/Ir is found. The total magnetic moment in the entire unit cell amounts to approximately ~4.5 μ_B for all chain configurations.

For all chains we have compared the total energy difference of the FM state and two antiferromagnetic (AFM) configurations: (i) parallel alignment of the Co moments of the two strands and antiparallel alignment along the chain and (ii) parallel alignment within each of the two strands and antiparallel alignment between the two strands. The obtained values clearly show the FM exchange coupling in the chains (see table 1). The FM exchange coupling is very strong along the chain independent of the chain structure. The strength of the FM coupling between the two strands, on the other hand, depends very much on the structure. While it is very strong for the C1 configuration with two close strands, the coupling is reduced by one order of magnitude for the C3 and C4 configurations. In contrast to the strong FM coupling along the Co chains, the exchange interaction is strongly influenced by the Fe/Ir hybridization for biatomic Fe chains on Ir(001) [12, 17]. This results in an AFM

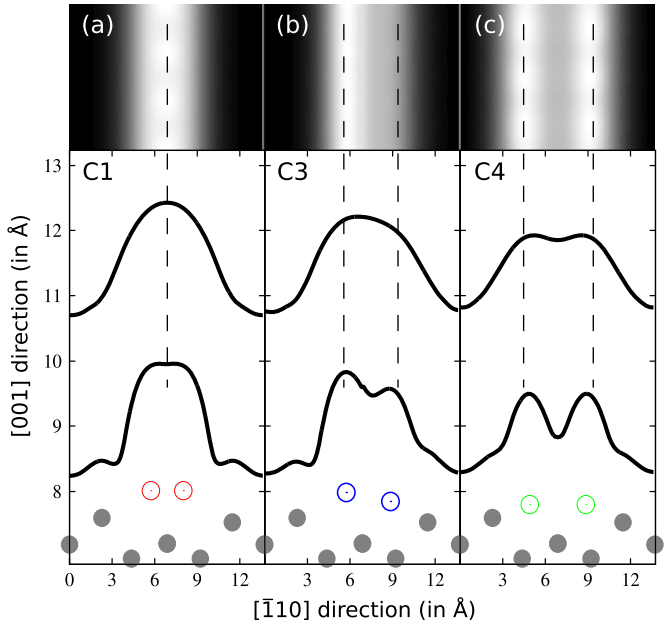

Figure 3. Simulated constant current STM images for a bias voltage of +0.1 V of (a) C1, (b) C3, and (c) C4 chains based on DFT calculations within the Tersoff–Hamann model. All images were obtained at a tip–surface distance of $z = 5.1$ Å. Line profiles at two different isovalues of the LDOS are shown below each image. At the bottom, the geometric arrangement of the Co chain atoms as well as the first Ir substrate layer are shown.

state for the C4 configuration [12], whereas in the C1 chains, the FM exchange interaction is weak and competes with the Dzyaloshinskii–Moriya interaction, leading to a spin-spiral ground state [17].

2.3. Simulated STM images

In order to directly compare our theoretical calculations with experiments, STM images were simulated for all chain types based on the Tersoff–Hamann model [26]. The local density of states (LDOS) has been integrated in an energy range of $[E_F;\ E_F + 100$ meV$]$ above the Fermi energy, E_F[5]. The images are shown in the upper panel of figure 3. For Co chains in the C1 configuration, the two strands cannot be distinguished in the image, figure 3(a), as they are separated by only 2.26 Å. On the other hand, for the C4 configuration in figure 3(c), the strands are separated by 4.10 Å allowing a clear distinction between them. The spacing between the two strands in the line profile depends on the distance from the surface due to the directionality of the decay of the electron density into the vacuum. In the C3 configuration, figure 3(b), the strands are separated by 3.18 Å. Due to the symmetry breaking in this zigzag chain configuration, an asymmetric image is obtained in which the strand in the IH site appears brighter.

For a comparison between theory and experiments, line profiles were obtained from the calculated vacuum LDOS. The lower panel of figure 3 shows constant LDOS line profiles for two different values, i.e., two different distances from the surface. From this figure, it can be confirmed that, for the C1 chain, even very close to the surface the two strands cannot be distinguished. For the C4 chain, on the other hand, the two strands can be clearly resolved. The C3 chain has an asymmetric corrugation profile and whether the two strands can be distinguished depends on the chosen value of the current, i.e., tip-sample separation.

2.4. Magnetocrystalline anisotropy

For the biatomic chains possessing mirror symmetries along and perpendicular to their axis, the easy axis of the magnetization can only lie along one of the high symmetry directions: out-of-plane (OP) to the surface, in-plane along the chain axis ([110] direction) and in-plane perpendicular to the chain axis ([$\bar{1}$10] direction) (see figure 1). The easy magnetization axis of the C1 chain, where the two strands are closest, is OP with energy differences of 0.17 meV/Co-atom and 0.40 meV/Co-atom with respect to the [110] direction and [$\bar{1}$10] direction. For the C4 chain, the easy axis is oriented along the chain axis and the hard axis is along the surface normal (1.00 meV/Co-atom) and the [$\bar{1}$10] direction is the intermediate state (0.59 meV/Co-atom). Qualitatively, the same results were found for biatomic Fe chains [12].

[5] Using occupied states in an energy range of $[E_F - 100$ meV; $E_F]$ leads to the same conclusions.

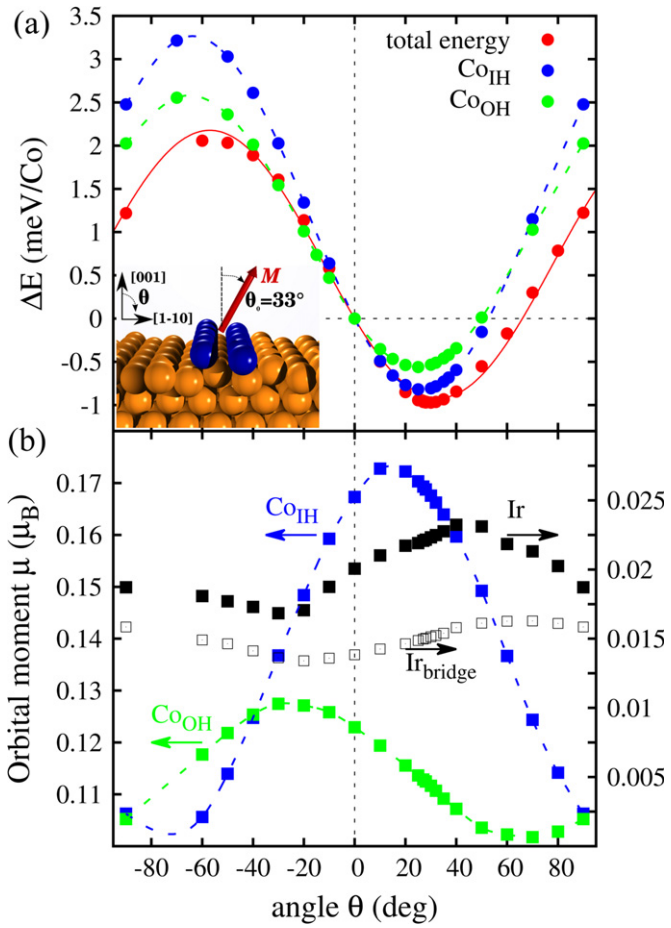

Figure 4. (a) MAE calculated for the zigzag (C3) Co chain. The SQA is rotated in a plane perpendicular to the chain axis as shown in the inset. Beside the total energy, calculations are shown in which SOC has been turned off in one of the two Co strands (Co_{IH}: SOC off in the OH strand and vice versa for Co_{OH}). The dotted lines represent a fit to the MAE according to uniaxial anisotropy expression. (b) Orbital moments of the two inequivalent Co atoms, all Ir atoms, and the bridge Ir atom.

Due to symmetry breaking, the situation becomes more complicated for the deposited zigzag (C3) chains and the easy magnetization direction does not need to align with a high symmetry direction, although it has to do so for the freestanding zigzag chain. The total energy was therefore calculated by rotating the spin quantization axis (SQA) also in a plane perpendicular to the chain axis. As can be seen in figure 4(a), a minimum of about 1 meV/Co-atom is obtained for an angle of $\theta_0 = 33°$ (see red curve).

In the spirit of the Bruno formula, which links the energy minimum to the maximum of the orbital moment [27], we can interpret this result based on the orbital contributions of individual atoms displayed in figure 4(b). Since the zigzag chain is composed of two non-equivalent strands, we observe different sizes and angular dependencies for the IH and OH Co atoms. While the maximum is at a positive angle of 15° for the IH Co strand, it is at −23° for the OH strand. This leads to an opposite preference of the favorable magnetization direction for the two Co atoms. In agreement, the calculated energy displays a minimum of $\theta \approx 0°$ if the SOC contribution of the entire substrate is not considered (not shown)[6].

The driving force behind the giant canting stems from interplay of the broken chain symmetry and the large Ir substrate contribution to the anisotropy of total energy and orbital moments. When the SOC contribution is considered in the substrate and in only one of the Co strands, we still acquire a total energy minimum at positives angles (figure 4(a)) irrespective of the considered Co strand. This shows that although one of the Co strands favors canting with a negative angle, its contribution is overwhelmed by that of the substrate. In agreement with the total energy, the maximum orbital moment of all Ir atoms in the first surface layer is found at a large positive angle of 44°. The main contribution to this orbital moment comes from the Ir atoms at the bridge site between the two Co strands (see figure 1). For each of the bridge Ir atoms the nearest neighbor Co atoms, which are different in their electronic structure due to different coordination, form a triangle with identical orientation.

[6] Note that the FM exchange coupling between the two Co strands is too strong to allow for a canting of the magnetic moments from each other. For a system with a weaker exchange coupling, however, such a non-collinear state could occur.

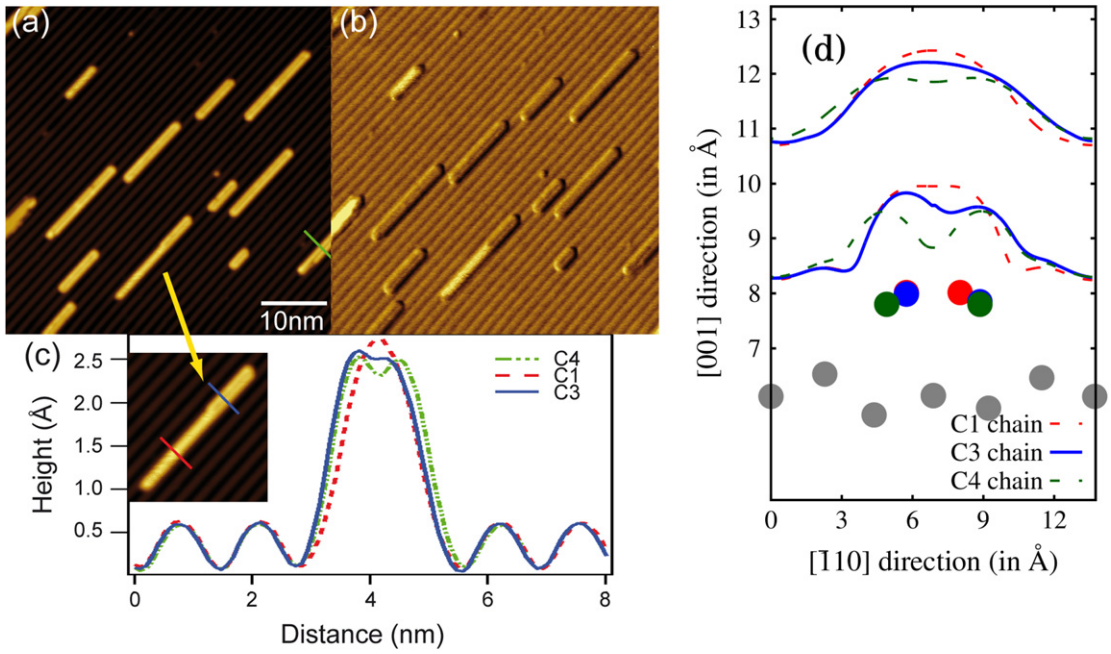

Figure 5. (a) STM topography image and (b) simultaneously obtained dI/dU image of Co chains on the (5 × 1) Ir(001) surface. (c) Line profiles of a C4 chain in image (a) and two profiles along a chain which changes structure along its axis from C1 to C3 (magnified in inset). Measurement parameters: W-tip, $T = 7.8$ K, $U_{bias} = -60$ mV, $I = 0.2$ nA. (d) Simulated line profiles of the three different chain types of figure 3 on a single graph.

This causes fundamental breaking of local symmetry, which results in all Ir bridge atoms favoring strong canting of magnetization towards a giant positive angle.

3. Experimental results

To confirm the predicted FM order and the canted magnetization of the zigzag Co chains we have performed spin-polarized STM (SP-STM) experiments [28]. Bulk Cr tips are used with an arbitrary magnetization direction that is not changed by the application of an external magnetic field.

3.1. Experimental details

The experiments were performed in a homebuilt cryogenic ultra high vacuum-STM with a base pressure of 10^{-11} mbar and a base temperature of $T = 7.5$–8.0 K [29]. The STM is placed in the center of a split coil magnet that can apply fields of up to $B = 2.5$ T normal to the sample surface (i.e., in the OP direction). All topographic STM images were taken in constant-current mode. Differential conductance (dI/dU) images were taken simultaneously with topography images by applying a small modulation to the bias voltage via a lock-in amplifier and capturing the resulting dI/dU signal with the same lock-in amplifier.

Samples were prepared by sputtering the Ir(001) surface and annealing to $T \approx 1600$ K for 1 min to achieve a clean, smooth surface with large terraces. The sample was cooled in vacuum to room temperature (30–90 min) and Co was deposited by electron bombardment heating of a 2 mm rod to evaporate material in a line of sight onto the Ir surface. Samples were transferred *in vacuo* to the STM where they were examined with polycrystalline W tips or bulk Cr tips, which were etched *ex situ*. W tips were flashed *in vacuo* to remove any adsorbed impurities. Bulk Cr tips were prepared *in vacuo* by field emission at $I = 50$ nA and $U = 300$ V for $t = 0.3$–2 h. The resulting Cr tips are magnetically sensitive with an arbitrary magnetization direction [31]. Due to their AFM nature, they do not react to magnetic fields.

3.2. Growth and structure

Figures 5(a) and (b) show STM topography and dI/dU images of Co deposited on the (5 × 1) reconstructed Ir (001) surface. As expected, wires form along the trench structure of the surface. Several contrast levels are present in the dI/dU image, indicating differences in the electronic structure, which demonstrates that multiple chain structures are present on the surface[7]. The chain configurations can be determined from line profiles

[7] The very bright chain on the middle left of the image is a lifted-reconstruction defect and can be ignored.

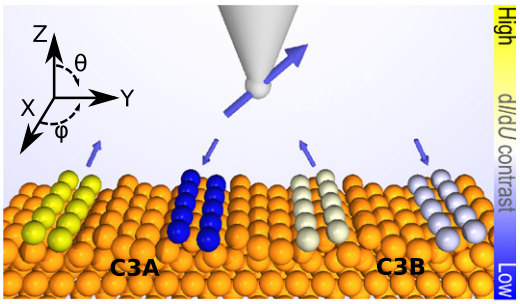

Figure 6. Sketch of a magnetic tip and the two types of zigzag chains with the OH site strand either on the right (C3A) or left (C3B). The easy axis is canted by 33° from the surface normal in the direction of the OH site atom, i.e. $\theta = \pm 33^\circ$ for C3A and C3B chains, respectively. The tip magnetization is chosen at $\theta = 50^\circ$.

shown in figure 5(c) taken perpendicular to the chains as marked in the inset and figure 5(a). Three different profiles can be distinguished: the dashed red curve shows a single peak with a narrow chain profile, the dot-dashed green curve shows a double peak with a wide chain profile, and the solid blue line shows a double peak with a profile that matches the narrow chain on the right and the wider chain on the left. When these three profiles are compared with the line profiles obtained from our DFT calculations based on the Tersoff–Hamann model [26] (figure 5(d)), the chains can be identified as C1, C4, and C3, respectively. We find about 80–95% of the Co atoms in C3 chains, 5–15% in C1 chains, and very few (< 5%) in C4 chains. A more detailed comparison demonstrates a good agreement of the geometries obtained from theory with the experimental result. At the edge of the unit cell all the simulated line profiles of figure 3 can be aligned. In figure 5(d), we see that up to the center of the left strand of the chain, the line profiles of the C1 and the C3 chain lie on top of each other, while the profile of the C4 matches that of the C3 chain from the center of the right strand. The perfect agreement between the line profiles of C1 and C4 configuration on the two strands of the C3 chain indicates that the IH and OH strands of the C3 chain are very similar to that of the respective symmetric chain type.

3.3. SP-STM experiments

The envisioned SP-STM experiment is sketched in figure 6: due to the symmetry of the sample two mirror-symmetric Co zigzag chains are expected on the reconstructed Ir(001) surface, each with two possible magnetization directions along the easy axis. Within the spin-polarized Tersoff–Hamann model [30], the tunneling current can be written as $I = I_0 + I_{SP}\mathbf{m}_T\mathbf{m}_S$ where the first and second term are the non-spin-polarized and spin-polarized contribution, respectively, and $\mathbf{m}_T$ and $\mathbf{m}_S$ are the unit vectors of tip and sample magnetization. Therefore, with a perfectly OP ($\theta = 0^\circ$) or in-plane magnetized tip ($\theta = 90^\circ$), only two contrast levels are measured. However, a suitable canted tip magnetization can in principle discern all four possible magnetization directions of the chains, as demonstrated for the tip sketched in figure 6. As the magnetization of the tip is close to the easy axis of one type of zigzag chains (left, C3A), there is a large positive (C3A, ↑) or negative (C3A, ↓) contribution from the spin-polarized current for the two magnetization directions leading to a high or low dI/dU signal, i.e., providing a high magnetic contrast. For the other type of zigzag chains (right, C3B), the projection of the tip magnetization onto the chain magnetization is much smaller leading to dI/dU signals that are closer in value. Depending on the exact tip angle and the noise in the experiment the variation of the dI/dU signal, i.e., magnetization direction, of the latter chain type will not be resolved and thus instead of a four-level contrast only a three-level contrast is obtained.

SP-STM measurements on six zigzag Co chains are shown in figure 7. The two mirror-symmetric chain configurations can be identified in the line profiles of the topography (a); while most chains exhibit a single configuration one chain in the image area changes from C3A to C3B at a defect. The virgin state dI/dU image in figure 7(b) exhibits either a very high (yellow) or comparably low (blue) signal for the C3A-chains, whereas the C3B-chains show a uniform intermediate (gray) signal. This uniform contrast level on each chain is indicative of FM order. The observation of a three-level contrast that is also visible in the line sections of figure 7(b) is in agreement with the considerations related to the sketch in figure 6 confirming a canted chain magnetization.

The application of an external magnetic field induces a magnetization reversal for the chains with antiparallel magnetization components: figure 7(c) shows that the three upper C3A-chains have turned into the same magnetization state as the C3A-chain on the lower left and they appear red in the difference image (d). The magnetic contrast for the C3B-chain is still in the intermediate state, leading to a two-level contrast in applied magnetic field, as seen in the right panel of figure 7(c). Although the exact magnetization angle cannot be

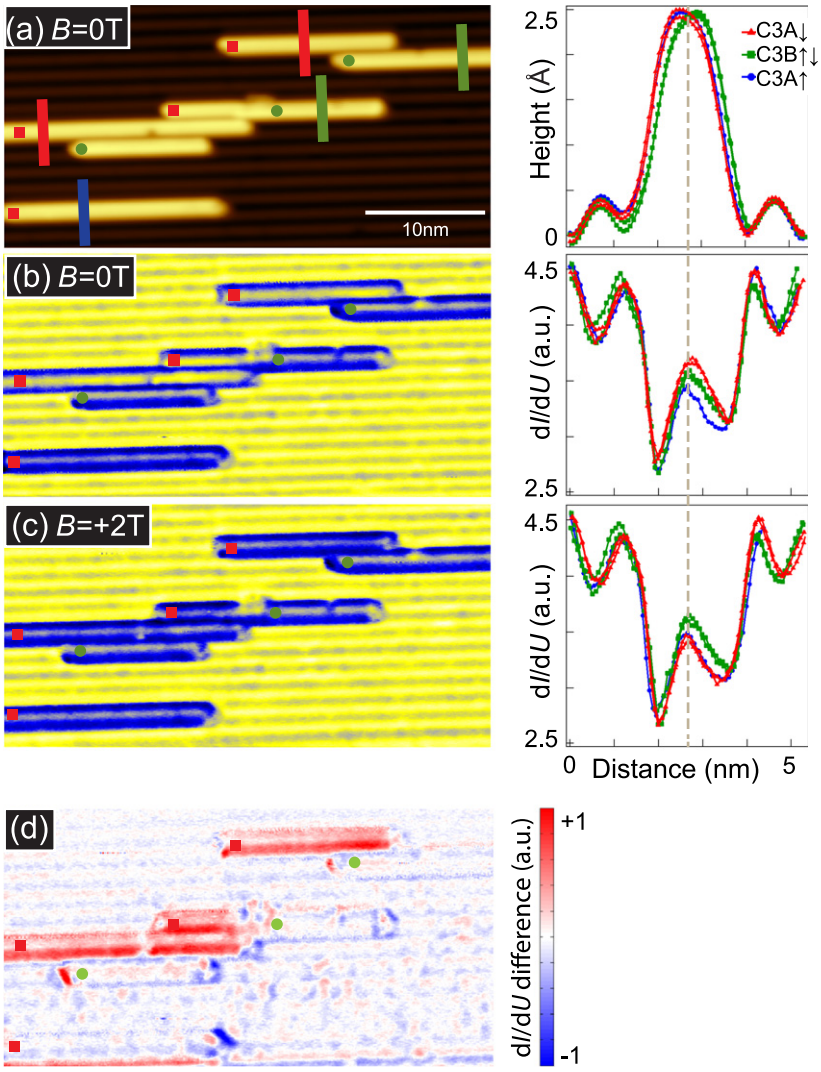

Figure 7. (a) SP-STM image of zigzag Co chains which have the strand in the OH site either on the upper (red squares, C3A) or on the lower side (green circles, C3B) of the chain (left). Line profiles as marked in the image showing the difference between C3A and C3B structures. (b), (c) Left panels show differential conductance images taken at $B = 0$ and +2 T respectively. Right panels display line profiles of the dI/dU signal taken at positions marked in (a) showing the contrast of the C3A and C3B chains with different magnetization directions. The dashed vertical line indicates the center of the chain. (d) Difference image of the two dI/dU maps (b) and (c). Measurement parameters: Cr-tip, $T = 7.5$ K, $U_{\text{bias}} = 300$ mV, $I = 3$ nA.

determined experimentally, we can conclude that the Co-chains are FM with a considerable canting of the magnetization away from the high-symmetry crystallographic axes, in agreement with the theoretical findings.

4. Conclusion

Our first-principles calculations based on DFT show that biatomic zigzag Co chains on the (5×1) reconstructed Ir(001) surface are FM and that their easy axis is canted from the surface normal by an angle of 33°. We explain that this very large effect is due to the local symmetry breaking of the bridge chain of Ir atoms in between the Co strands, which provides the dominant contribution to the MAE and favors large canting of the magnetization. Experiments performed using SP-STM confirm FM order at 8 K with a canted magnetization direction of the Co zigzag chains.

We have demonstrated that the local breaking of symmetry of the substrate due to proximity of an atomic chain can have a gigantic effect on the direction of the chain's magnetization which is not anticipated from intuitive symmetry arguments. Our results provide a direction for further advances in the area of control of complex low-dimensional magnets based on employing the reduced symmetry of nano-magnets at surfaces.

Acknowledgments

We thank Matthias Menzel, Gustav Bihlmayer, and Stefan Blügel for many fruitful discussions. JEB thanks the Alexander von Humboldt Foundation. YM gratefully acknowledges funding under the HGF-YIG programme VH-NG-513. SH thanks the Peter-Grünberg Institute of the Forschungszentrum Jülich for its hospitality during his stay. BD, YM, FO, and SH thank the HLRN, Jülich Supercomputing Centre, and RWTH Aachen University for providing computational resources and the DFG for financial support under project HE3292/8-1. JEB, AK, KvB, and RW are grateful to Matthias Menzel for experimental help and the DFG via SFB668-A8 and the ERC via the Advanced Grant FURORE for financial support.

References

[1] Gambardella P, Dallmeyer A, Maiti K, Malagoli M, Eberhardt W, Kern K and Carbone C 2002 *Nature* **416** 301
[2] Újfalussy B, Lazarovits B, Szunyogh L, Stocks G M and Weinberger P 2004 *Phys. Rev.* B **70** 100404
[3] Shick A B, Máca F and Oppeneer P M 2004 *Phys. Rev.* B **69** 212410
[4] Baud S, Ramseyer C, Bihlmayer G and Blügel B 2006 *Phys. Rev.* B **73** 104427
[5] Gambardella P, Dallmeyer A, Maiti K, Malagoli M, Rusponi S, Ohresser P, Eberhardt W, Carbone C and Kern K 2004 *Phys. Rev. Lett.* **93** 077203
[6] Baud S, Bihlmayer G, Blügel S and Ramseyer C 2006 *Surf. Sci.* **600** 4301
[7] Spišàk D and Hafner J 2003 *Surf. Sci.* **546** 27
[8] Spišàk D and Hafner J 2003 *Phys. Rev.* B **67** 214416
[9] Mokrousov Y, Bihlmayer G, Blügel B and Heinze S 2007 *Phys. Rev.* B **75** 104413
[10] Lounis S, Dederichs P H and Blügel S 2008 *Phys. Rev. Lett.* **101** 107204
[11] Mazzarello R and Tosatti E 2009 *Phys. Rev.* B **79** 134402
[12] Mokrousov Y, Thiess A and Heinze S 2009 *Phys. Rev.* B **80** 195420
[13] Hashemi H, Hergert W and Stepanyuk V S 2010 *Phys. Rev.* B **81** 104418
[14] Crain J N and Pierce D T 2005 *Science* **307** 703–6
[15] Erwin S C and Himpsel A J 2010 *Nat. Commun.* **1** 58
[16] Hirjibehedin C, Lutz C and Heinrich A 2006 *Science* **312** 1021
[17] Menzel M, Mokrousov Y, Wieser R, Bickel J E, Vedmedenko E, Blügel S, Heinze S, von Bergmann K, Kubetzka A and Wiesendanger R 2012 *Phys. Rev. Lett.* **108** 197204
[18] Loth S, Baumann S, Lutz C P, Eigler D M and Heinrich A J 2012 *Science* **335** 196
[19] Gilarowski G, Mendez J and Niehus H 2000 *Surf. Sci.* **448** 290
[20] Hammer L, Meier W, Schmidt A and Heinz K 2003 *Phys. Rev.* B **67** 125422
[21] www.flapw.de
[22] de Santis M, Gauthier Y, Tolentino H C N, Bihlmayer G, Blügel S and Langlais V 2007 *Phys. Rev.* B **75** 205432
[23] Perdew J P, Chevary J A, Vosko S H, JacksonK A, Pederson M R, Sing D J and Fiolhais C 1992 *Phys. Rev.* B **46** 6671
[24] Vosko S H, Wilk L and Nusair M 1980 *Can. J. Phys.* **58** 1200
[25] Liechtenstein A I, Katsnelson M I, Antropov V P and Gubanov V A 1987 *J. Magn. Magn. Mater.* **67** 65
[26] Tersoff J and Hamann D R 1983 *Phys. Rev. Lett.* **50** 1998
[27] Bruno P 1989 *Phys. Rev.* B **39** 865
[28] Wiesendanger R 2009 *Rev. Mod. Phys.* **81** 1495
[29] Pietzsch O, Kubetzka A, Haude D, Bode M and Wiesendanger R 2000 *Rev. Sci. Instrum.* **71** 424
[30] Wortmann D, Heinze S, Kurz P, Bihlmayer G and Blügel S 2001 *Phys. Rev. Lett.* **86** 4132
[31] Schlenhoff A, Krause S, Herzog G and Wiesendanger R 2010 *Appl. Phys. Lett.* **97** 083104